

RESEARCH ARTICLE

Adaptability evaluation of pavement structure to replacement treatment subgrade of black cotton soil

Yingcheng Luan¹, Yuan Ma^{1,2}, Weiguang Zhang^{1,*}, Yuqing Zhang^{3,4},
Tao Ma¹ and Jusang Lee⁵

¹School of Transportation, Southeast University, 2# Southeast University Road, Jiangning District, Nanjing 211189, China, ²Qilu Transportation Development Group, No. 1 Lg'ao West Rd, Lixia District, Jinan 250000, China, ³National Engineering Laboratory of Highway Maintenance Technology, Changsha University of Science & Technology, Changsha 410114, China, ⁴Aston Institute of Materials Research, Engineering Systems & Management Group, Aston University, Birmingham, B4 7ET, UK and ⁵Indiana Department of Transportation, West Lafayette, IN 47906, USA

*Corresponding author: wgzhang@seu.edu.cn

Abstract

Aiming at the typical engineering problem of black cotton soil (BCS) subgrade under the alternation of dry and wet climate in the region of Nairobi, Kenya, this paper takes the pavement structure as the research object, and the numerical calculation model of BCS subgrade is established based on the consolidation coupling theory of unsaturated soil. Taking the modulus and thickness of the subbase as variables, the deformation characteristics and additional stresses of different pavement structures are analysed. Then the adaptability of different pavement structures to replacement treatment subgrade of BCS is evaluated by gray incidence decision analysis method. The results show that whatever the pavement structure is, neither subgrade modulus nor thickness is sensitive to the pavement surface deformation, and the deformation differences between each pavement structure are more obvious in wet season; the additional stress at control layer bottom and pavement surface decreases with the increase of subbase modulus, whereas the stress may increase at subbase bottom; the additional stress at subbase bottom, control layer bottom and pavement surface all decreases with the increase of subbase thickness for pavement Structure I and II. For pavement Structure III, the change of subbase thickness is not sensitive to the additional stress at the control layer bottom and pavement surface, whereas the stress at subbase bottom increases with the increase of subbase thickness. It is concluded that the most adaptable structure

Received: December 29, 2019. Revised: February 8, 2020. Accepted: March 12, 2020

© The Author(s) 2020. Published by Oxford University Press on behalf of Central South University Press.

This is an Open Access article distributed under the terms of the Creative Commons Attribution Non-Commercial License (<http://creativecommons.org/licenses/by-nc/4.0/>), which permits non-commercial re-use, distribution, and reproduction in any medium, provided the original work is properly cited. For commercial re-use, please contact journals.permissions@oup.com

is pavement Structure I, which can minimize the comprehensive level of pavement settlement and additional stress.

Keywords: black cotton soil; pavement structure; numerical calculation; deformation; additional stress

1. Introduction

BCS is a kind of bad engineering geological soil with many cracks, over-consolidation and repeated swelling and contraction deformation characteristics generated by igneous rocks under extreme seasonal climate change. The mineral composition of BCS contains a large number of hydrophilic minerals. It swells after water absorption and shrinks after water loss with the deformation characteristics of repeated expansion and contraction, and belongs to typical expansive soil. It is common in the South Asian subcontinent, Australia and the central regions, eastern parts and south semi-humid areas of Africa. The BCS in eastern Africa is mainly distributed in countries such as Kenya, South Sudan, Ethiopia and Tanzania [1–6]. In the construction process of BCS subgrade highway in African, the pavement structure is usually designed according to the traffic level and climate conditions. However, in the later using phase, some typical pavement diseases occur, such as embankment or foundation settlement, subgrade cracking, pavement cracking, etc., which have a serious impact on the safety and quality of highway projects [7, 8, 9].

Many experts have studied the rational treatment methods of BCS subgrade. To improve the performance of BCS, many strengthening technologies, such as hydrated lime, ordinary Portland cement, petroleum sulfonate, asphalt and certain resins, have been employed with varied degrees of success [10–14]. Reddy *et al.* [15] studied that the lime-stabilized BCS is proportioned with brick powder to obtain the optimum mixture that yields a better CBR value, and it is promising to use this as subbase material in flexible pavements. Alhaji and Alhassan [16] treated BCS from Nigeria with 0–100% reclaimed asphalt pavement in 10% steps to evaluate the microstructure and strength of the compacted mixtures, and 30% RAP and 3.07% bitumen are adopted for the optimal mixture giving the highest strength. Yohanna *et al.* [17] evaluated a reliability estimate of bearing capacity values of cement-iron ore tailing treated BCS using a predictive model, then the cohesion, friction angle,

plasticity index, unit weight and compaction effort had a significant effect on the reliability index values. Chen *et al.* [18] studied compaction characteristics of BCS admixed at a different percentage of coir fibres with optimum lime content and without lime content, then the maximum dry density and optimum moisture content changed with the variation of fibre content and the alkali treatment of coir fibre can significantly improve the compaction characteristics and strength of BCS.

Industrial by-products/wastes such as fly ash, cement kiln dust, rice husk ash and the combination of these materials can bind soil particles together and reduce water absorption by clay particles [19]. Sani *et al.* [20] assess the suitability of BCS treated with locust bean waste ash mixtures as road pavement sub-base material, and more potent additives such as cement or lime are recommended to model optimum moisture content of compaction [21]. Gobinath *et al.* [22] investigated that the use of precipitated silica from the burning of rice husk can improve the geotechnical engineering properties of BCS by reducing its plasticity and making it more workable, improving its soaked strength, and increasing its permeability and the rate at which the soil gets consolidated [23]. Ikeagwuani *et al.* [24] investigated the effects of different sawdust and lime mixtures on the mechanical properties of BCS, and the optimum mixture content with 16% sawdust ash and 4% lime is proposed that can maximize enhance its strength [25]. Patel *et al.* [26] investigated the effects of dolime content and curing period on the basic geotechnical properties of the BCS in the subbase course of flexible pavements, and developed empirical relationships to estimate important design parameters and resilient modulus [27]. Jimoh *et al.* [28] studied the strength properties of BCS subgrade modified with quarry fines were stabilized with cement kiln dust and achieved desired performance in road pavement subgrades [20]. The above mainly studies the treatment methods of the BCS subgrade, which can improve its mechanical strength and minimizes the deformation, then satisfactory results are

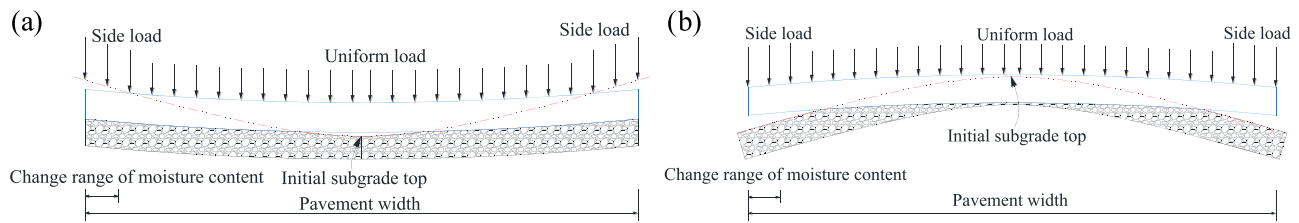


Fig. 1. Failure modes caused by expansion and contraction deformation of subgrade: (a) Roadside heave; (b) Roadside settlement

Table 1. Pavement structure design

Structure	Structure I	Structure II	Structure III
Total thickness	600 mm	630 mm	660 mm
Surface course	50 mm: fine aggregate asphalt concrete 100 mm: dense-graded asphalt macadam 50 mm: anti-fatigue layer	30 mm: fine aggregate asphalt concrete 50 mm: middle aggregate asphalt concrete 100 mm: dense-graded asphalt macadam	40 mm: fine aggregate asphalt concrete 60 mm: middle aggregate asphalt concrete
Base course	200 mm: graded macadam 200 mm: cement stabilized macadam	150 mm: cement stabilized macadam 150 mm: graded macadam 150 mm: cement stabilized macadam	360 mm: cement stabilized macadam 200 mm: cement soil

obtained. However, there are many reasons for the asphalt pavement diseases in the BCS area [29–32]. On the one hand, the insufficient subgrade strength can cause post-construction settlement or uneven settlement; on the other hand, the reason is that the designs of pavement structures and materials are unreasonable. From the point of view of the asphalt pavement structure, a feasible pavement structure design method is proposed according to the characteristics of BCS [33–36].

Three typical pavement structures are selected in this paper. Based on the consolidation coupled theory of unsaturated soil, a numerical model of pavement structure of BCS subgrade with replacement treatment is established, and meteorological data of a dry-wet cycle in Nairobi is taken as boundary conditions. Then the deformation characteristics of different pavement structures and additional stresses of each structure layer are analysed. Aiming at surface deformation and additional stress, the adaptability of different pavement structures to BCS subgrade with replacement treatment is evaluated by gray incidence decision analysis methods.

2. Methodology

2.1. Engineering background

The southern ring road of Nairobi in Kenya is 28.6 km long, and it is a two-way four-lane road. The starting point is at the intersection with

Mombasa Road and the ending point is connected to KabeteLimum Road near Kikuyu Town. The traffic type is T1 and the standard pavement structure type is T11.

This section is the BCS distribution area under natural conditions, and the climate alternates obviously in dry and wet seasons. This can lead to water swelling in the wet season and drying shrinkage in the dry season for the BCS in the outside of subgrade. Under the action of external load and self-weight of the pavement structure, the pavement structure repeatedly appears the phenomenon of roadside settlement or heave as shown in Fig. 1, which causes the bottom of the base layer and the pavement surface to be repeatedly in tension state and be very vulnerable to crack. This has become a key problem that needs to be solved urgently in the process of local road construction.

2.2. Design scheme of the pavement structure

Based on the above problems, aiming at the physical characteristics of BCS in this kind of environment, the authors take the pavement structure as the research object, and the applicability of different pavement structures to replacement treatment of BCS subgrade is studied. Compared with the conventional pavement structure, the authors emphatically consider that the pavement in the BCS distribution area may have a larger

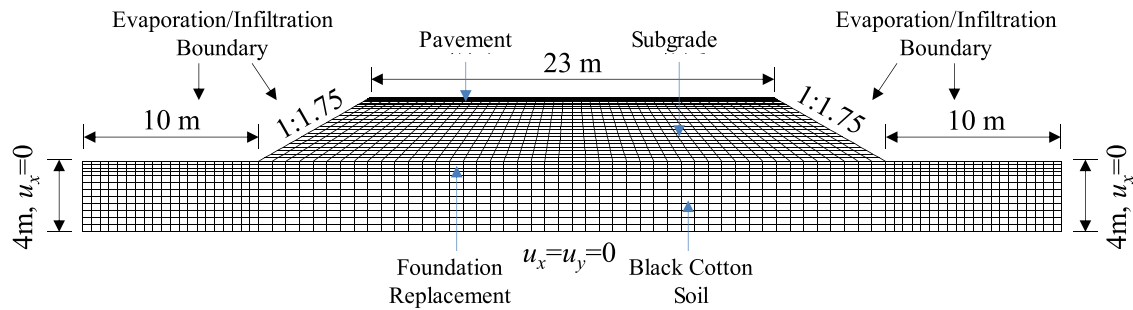


Fig. 2. Schematic diagram of the FEM model

non-uniform expansion and contraction deformation after the completion of pavement. Then, three kinds of pavement structure are designed, and the traditional semi-rigid base pavement structure is taken as the third scheme to make comparative analysis [37–39]. The specific scheme is shown in Table 1.

Structure I: asphalt concrete layer (including asphalt concrete, asphalt macadam, anti-fatigue layer) + graded macadam base + cement stabilized macadam subbase;

Structure II: asphalt concrete layer (including asphalt concrete and asphalt macadam layer) + cement stabilized macadam + graded macadam + cement stabilized macadam subbase;

Structure III: asphalt concrete layer + cement stabilized macadam base + cement soil subbase.

2.3. Construction of FEM model

2.3.1. Numerical model. In this paper, ABAQUS software is adopted for numerical calculation, and the size and shape of FEM are consistent with the typical cross-section of Nairobi South Ring Road. The width of the pavement is 23 m, and the height of the subgrade is 3 m; and the slope gradient is 1:1.75. According to the actual project, the thickness of the BCS layer is 4 m, and the replacement treatment is adopted to improve the bearing capacity of subgrade. White soil is a high-quality subgrade filling with the characteristic of high strength, so it is selected as the replacement material; and the replacement thickness is 0.8 m. The model element division and boundary conditions are shown in Fig. 2.

Based on the volume change theory of saturated-unsaturated soil, a modified thermal-mechanical coupling method is used to simulate and analyse the hydraulic coupling problem of the BCS. The 4-node thermal-mechanical coupling element CPE4T is selected for the foundation and subgrade fill, and the pavement structure is simulated by using 4-node plane-strain element CPE4.

2.3.2. Mechanical parameters..

(1) **Soil parameters.** Fredluad and Rahardjo [40] established the two-variable theory to describe the volume changing behaviour of saturated-unsaturated soil [22]. The constitutive relationship between state variables and stress state variables is defined; the state variables are void ratio, water content and saturation, and the two independent stress state variables are normal stress and matrix suction. In the case of known stress state variables, soil parameters, including elasticity modulus, expansion coefficient, specific water capacity, variation coefficient of water content related to normal stress and permeability coefficient of unsaturated soil, can be calculated by the obtained state variables.

The main program and four user subroutines are used in the whole numerical calculation. The main program defines the mesh generation, initial conditions, boundary conditions and analysis steps. The user subroutines carry out parameter calculation, seepage calculation, updating stiffness matrix and stress variables of saturated-unsaturated BCS.

According to the measured water content of BCS at specific buried depth, as shown in Fig. 3a, the matric suction of specific buried depth is calculated as shown in Fig. 3b; and the value of random buried depth is obtained by interpolation. The optimum water content of the replacement material is taken as the initial water content, and the corresponding matric suction is 1966 kPa.

(2) **Material parameters of surface course and base course.** In addition to graded macadam, other structural layers of pavement are assumed to be uniform, isotropic elastic and obey Hooke's law. The material parameters of each structural layer of Structure I, Structure II and Structure III are shown in Table 2.

In order to analyse the influence of different subbase modulus on the surface deformation of BCS caused by rainfall/evaporation, the subbase modulus (cement stabilized macadam) of the

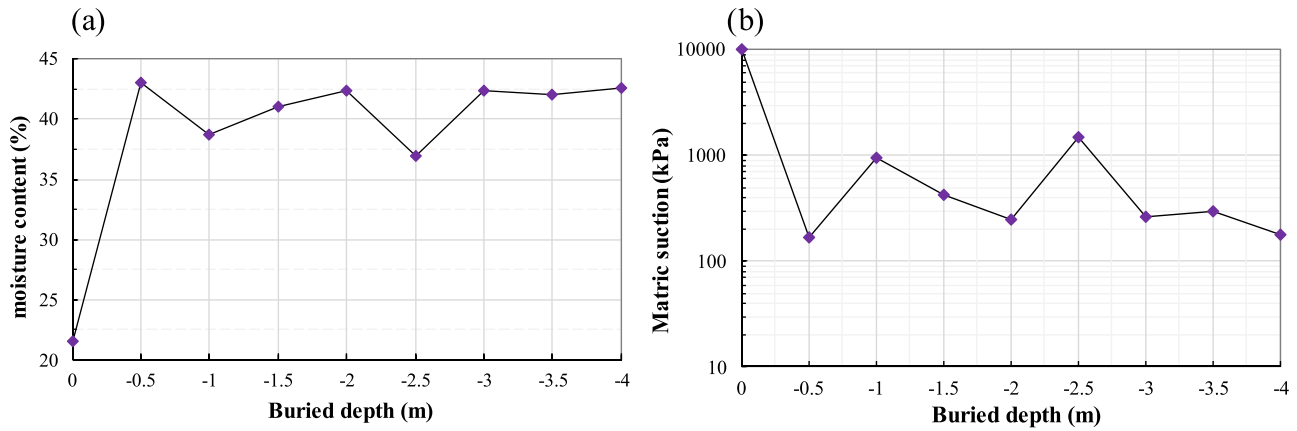


Fig. 3. Soil parameters (a) Curve of moisture content-buried depth; (b) Curve of matric suction-buried depth

Table 2. Design parameters of pavement structural materials

Material	Compressive modulus of 20°C (MPa)	Compressive modulus of 15°C (MPa)	Splitting strength of 15°C (MPa)	Poisson ratio
Fine-grained asphalt concrete	1400	2000	1.4	0.25
Medium-grained asphalt concrete	1200	1800	1.0	0.25
Dense asphalt concrete	120	1400	0.8	0.25
Anti-figure layer	1400	2000	1.4	0.25
Cement stabilized macadam	1500	1500	0.6	0.25
Soil-cement	550	550	0.25	0.25
Graded macadam	400	400	/	0.35

Structure I and Structure II are 1000, 1500 and 2000 MPa, respectively, and that of the Structure III are 300, 550 and 800 MPa, respectively.

2.3.3. *Grading macadam.* The residue modulus of granular material typically increases with the increase of stress magnitude. Such a relationship in most cases is non-linear and can be characterized in the equation below. Such non-linear property can be achieved in ABAQUS by extracting the three stresses within each analysis step by using subroutines. The K_1 and K_2 were set as 24 432 and 0.47 as recommended [24, 26, 28, 40–42].

$$E = K_1 \theta^{K_2}, \tag{1}$$

where E is the elastic modulus of grading macadam base; θ is the first stress invariant, and is a summation of the principle stresses σ_1, σ_2 and σ_3 , or the summation of normal stresses σ_x, σ_y and σ_z ; K_1 and K_2 are regression coefficients.

2.3.4. *Boundary conditions.* The horizontal displacement and vertical displacement of the bottom of the model and the horizontal displacement of the left and right sides of the boundary are limited. The

slope surface and the subbase surface are given to boundary condition of infiltration and evaporation, the evaporation intensity is 5×10^{-8} m/s, and the left and right sides of the model are the non-drainage boundary.

According to the meteorological data of Nairobi, such as atmospheric temperature, dew point temperature, and wind speed, the surface evapotranspiration is calculated by FAO56 Penman-Montieth formula, and the calculation results are shown in Fig. 4a. See Fig. 4b for rainfall in Nairobi area from 13 July to 13 December 2016. It can be seen from Fig. 4 that July to October in Nairobi area is the dry season with less rainfall, followed by a rainy season of up to 2–3 months. Rainfall infiltration and surface evapotranspiration are applied to the slope surface and subbase surface of BCS by user subroutine.

3. Results and analysis

3.1. Effect of subbase parameters on pavement settlement and additional stress

3.1.1. *Effect of subbase modulus and thickness on pavement surface deformation.* Fig. 5a and b shows the effect of subbase modulus on the deformation of pavement surface during the dry season and wet season.

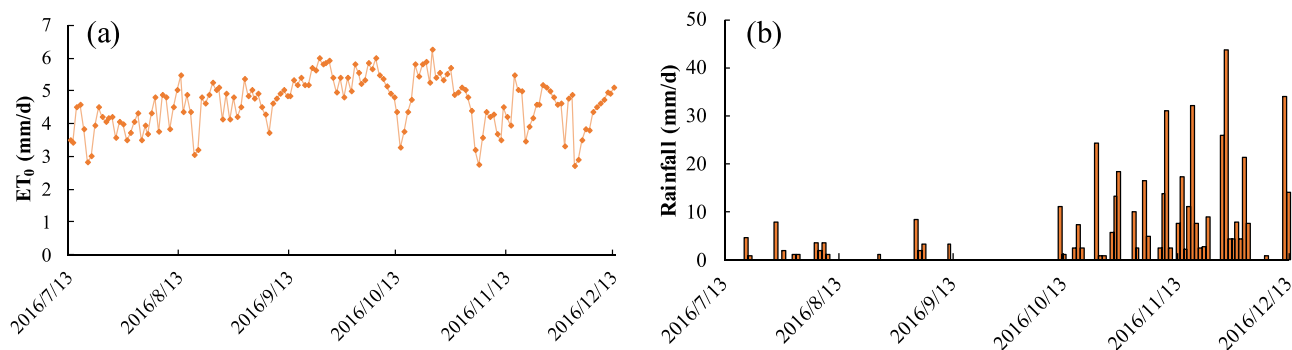


Fig. 4. Nairobi's climate of rainfall: (a) Reference evapotranspiration; (b) rainfall

When the subgrade of BCS shrinks after water loss in dry season, the surface settlement tends to decrease with the increase of the modulus of the subbase, but the decreasing extent is small. Similarly, the heave deformation of the pavement surface is basically unchanged between different subbase modulus in the wet season, and the small deformation differences only exist in the central region of Fig. 5b. Fig. 6c and d shows the influence of the subbase thickness on the pavement deformation. The overall deformation differences of different subbase thickness are similar to that of subbase modulus; and in the wet season, the small deformation differences between each scheme exist near the middle of the road, which is different from the subbase modulus variation. It is noted that the deformation of pavement surface is not sensitive to modulus and thickness variation of subbase (cement stabilized macadam) for both dry season and wet season.

As for the deformation trend of along the cross-section, the surface deformation keeps decreased in the wet season, and its decreasing rate gradually increases with the increase of the distance from the middle of the road; whereas the surface deformation decreases firstly and tends to become flat in the dry season.

The effect of pavement Structure II and pavement Structure III are also evaluated, and the relationships between subbase modulus/thickness and pavement surface deformation follow the same trend as that in Fig. 5, whereas the minor differences of numerical values exist in local locations of the curve.

3.1.2. Effect of subbase modulus and thickness on uneven pavement surface deformation. Fig. 6a and b shows the effect of subbase modulus on the uneven deformation of the pavement surface. As is shown in this figure,

the increase of subbase modulus may not affect the uneven pavement surface deformation in the dry season. However, the uneven deformation will present a slight growth trend with the increase of subbase modulus in the wet season. Therefore, the subbase modulus is not the critical factor for the uneven pavement surface deformation, and the average design modulus of 1500 MPa can be adopted in the pavement structure design.

The uneven deformation curve among subbases thickness of 15, 20 and 25 cm is shown in Fig. 6c and d. As seen, the uneven deformation is increased by 5.2%, as the thickness of subbase increasing from 15 to 25 cm. Thus, it is not wise to employ too thick subbase and the reasonable thickness is between 15 and 20 cm.

The effect of the subbase thickness and modulus of Structure II and Structure III on uneven deformation share a similar trend with the Structure I, whereas there are differences in deformation between different schemes. Specifically, compared with Structure I, the range of uneven pavement surface deformation increases by 5.8 and 5.1% for Structure II and Structure III when the subbase thickness increases from 15 to 25 cm, respectively.

3.1.3. Effect of subbase modulus and thickness on horizontal additional stress. The uneven settlement or heave of BCS subgrade will produce additional stress to the pavement structure, which will accelerate the damage of the pavement structure. Therefore, the following will focus on the analysis of the maximum horizontal additional stress of the base layer bottom, stress control layer bottom and pavement surface with the change of the subbase modulus and thickness in different pavement structures. The stress control layers of three kinds of pavement structure are anti-fatigue layer, cement stabilized macadam layer and cement stabilized macadam layer respectively.

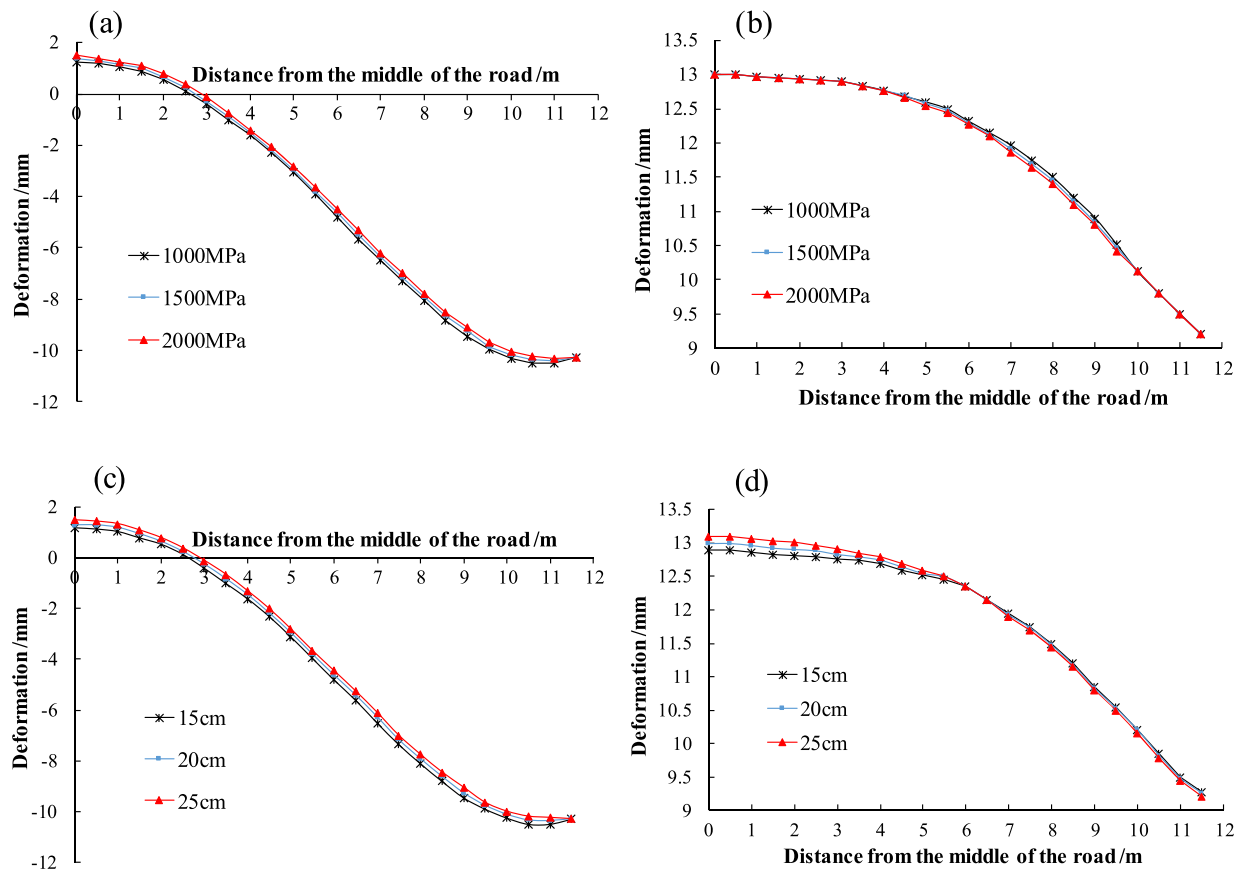


Fig. 5. Effect of subbase modulus and thickness on pavement surface deformation: (a) Subbase modulus variation (dry season, 2016-10-01); (b) Subbase modulus variation (wet season, 2016-12-01); (c) Subbase thickness variation (dry season, 2016-10-01); (d) Subbase thickness variation (wet season, 2016-12-01)

The subbase modulus of Structure I and Structure II are 1000, 1500 and 2000 MPa, respectively, and the subbase modulus of Structure III is 300, 550 and 800 MPa, respectively. Then the thickness is 15, 20 and 25 cm for all three kinds of pavement structure, respectively.

Structure I. The summaries of the effect of subbase modulus and thickness on horizontal additional stress at the subbase layer bottom, stress control layer bottom and pavement surface are presented in Fig. 7a and b. Fig. 7a indicates that the horizontal additional stress at subbase bottom increases with the increase of subbase modulus, whereas the horizontal additional stress at pavement surface and control layer bottom decreases with the increase of subbase modulus.

The reason may be the nonlinear characteristic of grading aggregate can be fully developed over the high modulus subbase. Therefore, the additional stress generates by uneven deformation can be partially absorbed, which can help reduce the tensile stress at the anti-fatigue layer bottom. Similarly, the additional stress decreases with the

increase of the subbase modulus at pavement surface.

Fig. 7b shows that the horizontal additional stress decreases with the increase of subbase thickness, and the effect of subbase thickness on the horizontal additional stress is not as sensitive as that of subbase modulus, especially for subbase bottom and control layer bottom.

Structure II. In Fig. 7c, it can be seen that the maximum horizontal additional stress at the control layer bottom and pavement surface decreases with the increase of the subbase modulus. It can be concluded that setting a higher subbase modulus is beneficial to reduce the cracking risk of the control layer and pavement surface. However, the increase of the subbase modulus will lead to an increase of the maximum additional stress at the subbase bottom. Therefore, 1500–2000 MPa is suitable for the subbase modulus.

In Fig. 7d, the maximum horizontal additional stress at the subbase bottom, the control layer bottom, and pavement surface decreases with the increase of the subbase thickness, especially

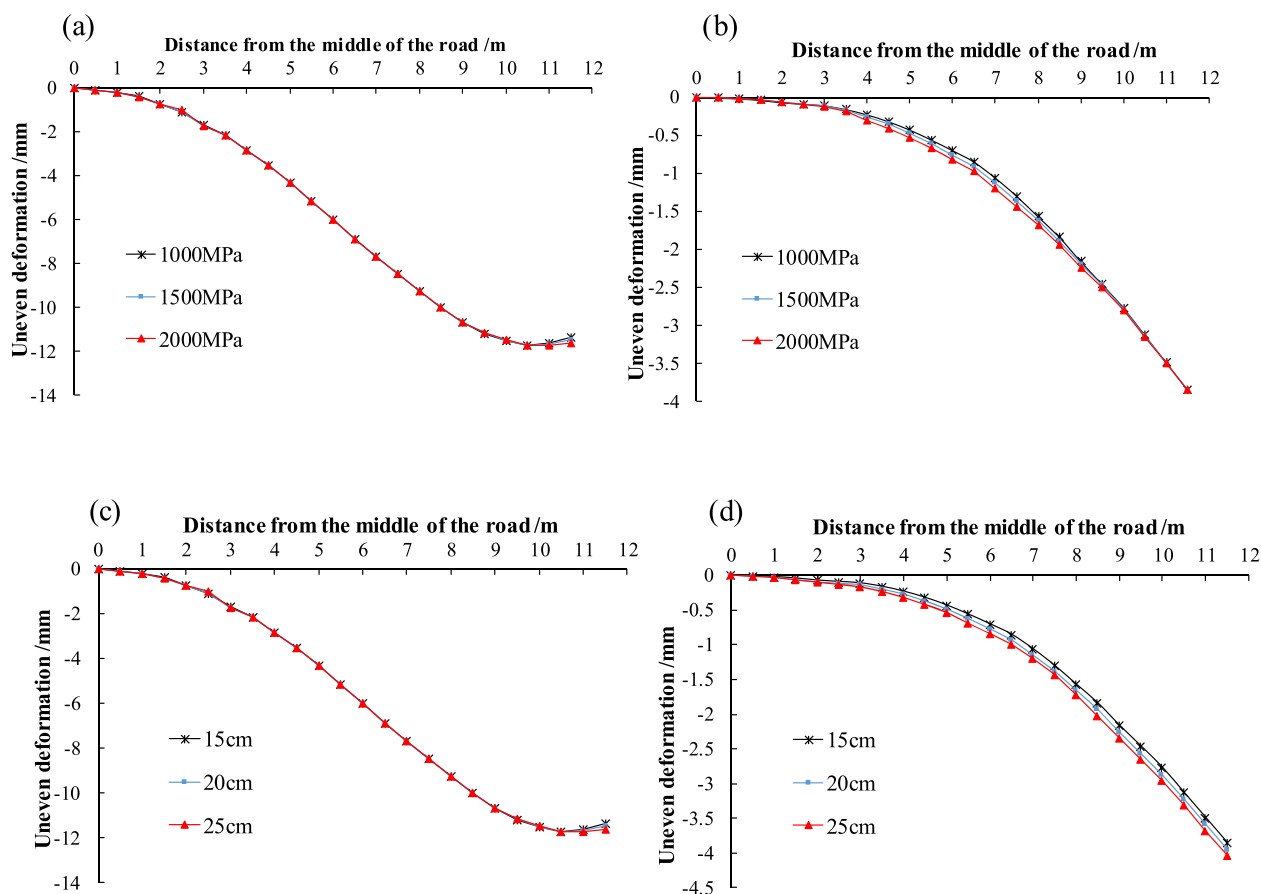


Fig. 6. Effect of subbase modulus and thickness on uneven pavement surface deformation: (a) Subbase modulus variation (dry season, 2016-10-01); (b) Subbase modulus variation (wet season, 2016-12-01); (c) Subbase thickness variation (dry season, 2016-10-01); (d) Subbase thickness variation (wet season, 2016-12-01)

the latter two are more obvious. Therefore, the increase of the subbase thickness is conducive to reducing the risk of pavement structure cracking due to the expansion and contraction deformation of the BCS foundation. As the excessive thickness of the pavement structure will also lead to a significant increase in project cost, it is more appropriate to use the subbase thickness of the 20–25 cm.

Structure III. It is shown in Fig. 7e that the trend of maximum horizontal additional stress at subbase bottom, control layer bottom and pavement surface of Structure III is similar to that of Structure I and Structure II with the change of the subbase modulus, whereas the value of subbase bottom has a relatively faster growth rate. Because of the importance of the control layer and the surface layer, the subbase modulus can be adopted by the 550 MPa.

As for the subbase thickness shown in Fig. 7f, the changing trend has little effect on the control layer bottom and pavement surface, but the subbase bottom is quite different from the first two pavement structures and its values increase with

the increase of the subbase thickness. Therefore, the design thickness of the subbase can adopt the design thickness, which is 20 cm.

3.2. Adaptability analysis of pavement structure

As regards the adaptability of different pavement structures on replacement treatment subgrade of BCS, it mainly refers to the pavement surface deformation, the uneven pavement surface deformation, the additional stress at subbase bottom, control layer bottom and pavement surface. These five indices are required to be evaluated before identifying the adaptability of three pavement structures on the treated subgrade of BCS. Considering the significant difference among the value and dimension of these indices, the gray incidence decision method is selected for the adaptability assessment.

In this section, in consideration of the pavement surface deformation characteristics, the maximum deformation difference and the maximum uneven deformation difference are adopted. Regarding the

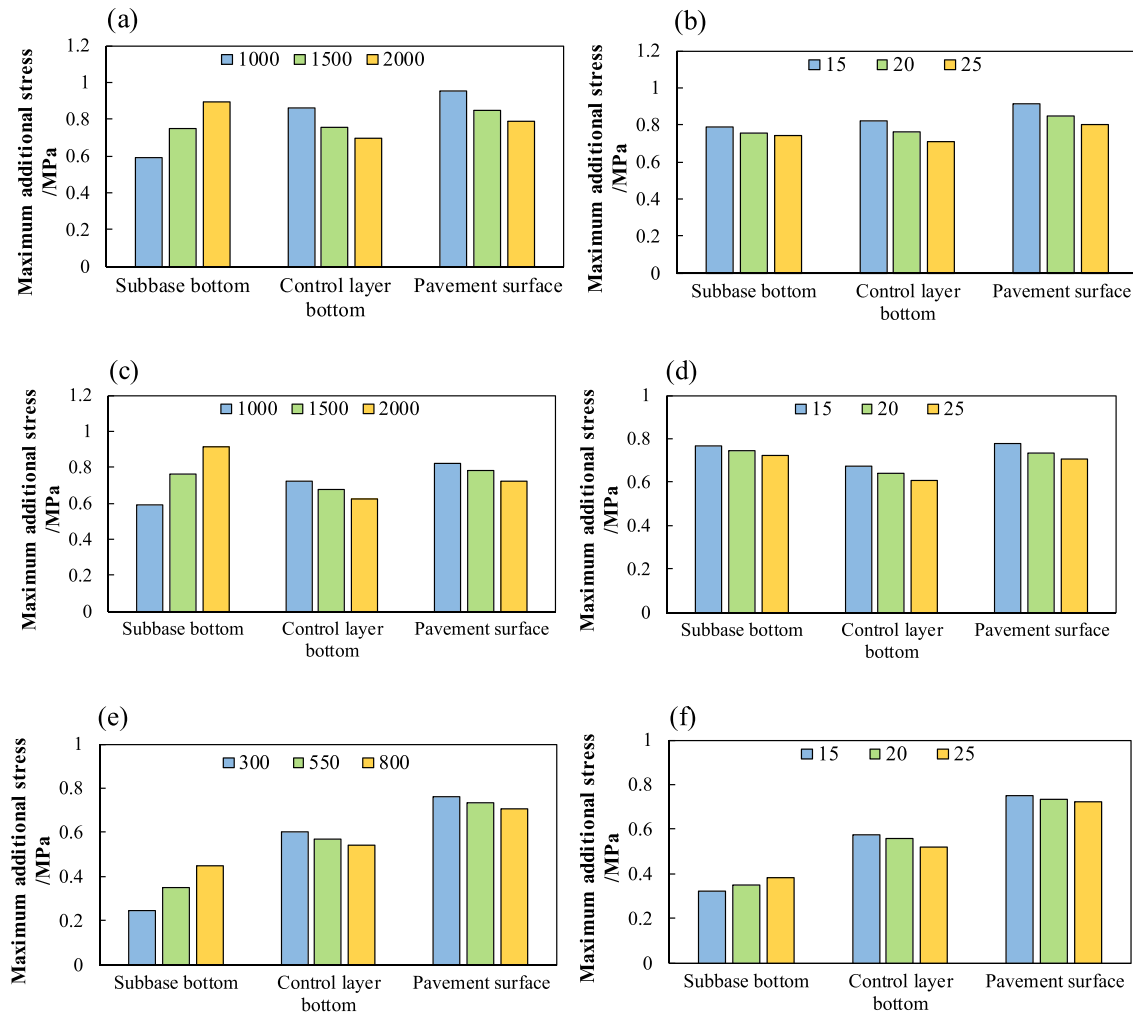


Fig. 7. Variation of additional stress with the change of subbase modulus and subbase thickness: (a) Additional stress-modulus (structure I); (b) Additional stress-thickness (structure I); (c) Additional stress-modulus (structure II); (d) Additional stress-thickness (structure II); (e) Additional stress-modulus (structure III); (f) Additional stress-thickness (structure III)

additional stress, strength action rate (abbreviated ‘SAR’, the ratio of additional stress to ultimate tensile strength) is adopted to be the comparative index.

- (1) Computational results of five objectives
 Define the adaptability of replacement treatment of BCS as event a_1 , then $A = \{a_1\}$; define the pavement Structure I as event b_1 , the pavement Structure II as event b_2 and the pavement Structure III as event b_3 , and the $B = \{b_1, b_2, b_3\}$. Then, the situation set is obtained as follows:

$$S = \langle S_{ij} = (a_i, b_i) \mid a_i \in A, b_i \in B \rangle = \langle S_{11}, S_{12}, S_{13} \rangle \tag{2}$$

Define the maximum deformation difference of pavement surface as target I, the maximum

uneven deformation difference of pavement surface as target II, the horizontal additional peak stress (SAR) of pavement surface, control layer bottom and subbase bottom as target III, target IV and target V respectively. Then the computational results are shown in Table 3.

- (2) The weight of five targets
 With respect to the pavement structure on the replacement treatment subgrade of BCS, the primary concern is the uneven deformation. Then, it is required to minimize the additional stress at the control layer bottom and pavement surface, which is represented by SAR. After that, surface deformation ought to be decreased in the operation process. Finally, the additional stress at the subbase bottom ought to mitigate the impact of uneven deformation on the upper structure. The weight of five targets can be acquired in Table 4.

Table 3. The results of five targets of the pavement structure

Target	Structure I	Structure II	Structure III
Target I: Maximum deformation difference	20.56	20.41	20.42
Target II: Maximum uneven deformation difference	15.49	15.62	15.80
Target III: SAR of pavement surface (%)	60.7	55.3	52.4
Target IV: SAR of control layer bottom (%)	54.4	112.2	94.2
Target V: SAR of subbase bottom (%)	126.7	127	138.8

Table 4. The weight of five targets

Target	Maximum deformation difference	Maximum uneven deformation difference	SAR of pavement surface	SAR of control layer bottom	SAR of subbase bottom
Weight	0.32	0.16	0.22	0.22	0.08

Table 5. The situation effect sequences

$u^{(1)}$	0.161	0.160	0.160
$u^{(2)}$	0.317	0.320	0.323
$u^{(3)}$	0.238	0.217	0.205
$u^{(4)}$	0.138	0.284	0.238
$u^{(5)}$	0.077	0.078	0.085

Table 6. The effect vectors

u_{11}	0.161	0.317	0.238	0.138	0.077
u_{12}	0.160	0.320	0.217	0.284	0.078
u_{13}	0.160	0.323	0.205	0.238	0.085

- (3) The situation effect sequences under η_k k target (mean value) $u^{(k)}$ ($k=1, 2, 3, 4, 5$) are obtained in Table 5.
- (4) The effect vectors u_{ij} for situation S_{ij} ($i=1; j=1, 2, 3$) are acquired in Table 6.
- (5) According to the principle that the value of each target should be kept as small as possible, the lower values of each target are $u_{i0j0}^{(1)} = \min \{u_{ij}^{(1)}\} = 0.160$, $u_{i0j0}^{(2)} = \min \{u_{ij}^{(2)}\} = 0.317$, $u_{i0j0}^{(3)} = \min \{u_{ij}^{(3)}\} = 0.205$, $u_{i0j0}^{(4)} = \min \{u_{ij}^{(4)}\} = 0.318$, $u_{i0j0}^{(5)} = \min \{u_{ij}^{(5)}\} = 0.077$, respectively. Thus, the ideal optimal effect vector is $u_{i0j0} = \{0.160, 0.317, 0.205, 0.138, 0.077\}$.

The absolute gray incidence degrees between u_{ij} and u_{i0j0} are ε_{ij} ($i=1; j=1, 2, 3$). Therefore, $\varepsilon_{11}=0.978$ (Structure I), $\varepsilon_{12}=0.894$ (Structure II), $\varepsilon_{13}=0.920$ (Structure III).

It is indicated that the adaptability of pavement Structure I is the best, then following pavement Structure III and pavement Structure II is the least adaptable structure.

4. Conclusions

This paper evaluated the different deformation characteristics and additional stress characteristics of BCS treated subgrade using three pavement structures. The gray incidence analysis method was utilized to evaluate the adaptability of three pavement structures. The major conclusions are as follows:

- (1) For BCS treated subgrade, whatever the pavement structure is, neither subgrade modulus nor subgrade thickness is sensitive to the pavement surface deformation. The uneven

settlement and upheaval on pavement surface increased with the increase of subbase modulus and subbase thickness, whereas the increasing extent is limited; and the deformation differences between each pavement structure are more obvious in the wet season.

- (2) Regardless of pavement structures, the additional stress at the control layer bottom and pavement surface decreased with the increase of subbase modulus, whereas the stress may increase at subbase bottom.
- (3) For pavement Structure I and II, the additional stress at subbase bottom, control layer bottom, and pavement surface all decreased with the increase of subbase thickness. For pavement Structure III, the change of subbase thickness was not sensitive to the additional stress at the control layer bottom and pavement surface, whereas the stress at subbase bottom increase with the increase of subbase thickness.
- (4) The most adaptable structure is pavement Structure I, which sets the anti-fatigue layer. This type of pavement can minimize the comprehensive level of pavement settlement and additional stress.

Acknowledgements

This research was funded by the National Natural Science Foundation of China, grant number 51878164 and 51922030, Southeast University "Zhongying Young Scholars" Project, and Department of Transportation of Shandong Province, grant number 2018B51.

Conflict of interest statement. The authors have declared that no conflict of interest exists.

References

1. Ackroyd LW, Husain R. Residual and lacustrine black cotton soils of north-East Nigeria. *Geotechnique* 1986; **36**:113–8.
2. Behrensmeyer AK, Potts R, Plummer T, et al. The pleistocene locality of kanjera, western Kenya - stratigraphy, chronology and paleoenvironments. *J Hum Evol* 1995; **29**:247–74.
3. DE VOS t. N.C JH, Virgo KJ. Soil structure in vertisols of the Blue Nile clay plains, Sudan. *Eur J Soil Sci* 1969; **20**: 189–206.
4. Deocampo DM. Authigenic clays in East Africa: regional trends and paleolimnology at the Plio–Pleistocene boundary, Olduvai Gorge, Tanzania. *J Paleol* 2004; **31**:1–9.
5. Kanyanjua SM, Keter JK, Okalebo RJ, et al. Identifying potassium-deficient soils in Kenya by mapping and analysis of selected sites. *Soil Sci* 2006; **171**:610–26.
6. Mees F, Stoops G, Van Ranst FM, et al. The nature of zeolite occurrences in deposits of the olduvai basin, northern Tanzania. *Clays Clay Miner* 2005; **53**:659–73.
7. Ding XH, Ma T, Gu LH, et al. Investigation of surface micro-crack growth behaviour of asphalt mortar based on the designed innovative mesoscopic test. *Mater Design* 2020a; **185**:108238.
8. Ma T, Zhang DY, Zhang Y, et al. Effect of air voids on the high-temperature creep behavior of asphalt mixture based on three-dimensional discrete element modeling. *Mater Design* 2015a; **89**:304–13.
9. Ma T, Wang H, Zhang DY, et al. Heterogeneity effect of mechanical property on creep behavior of asphalt mixture based on micromechanical modeling and virtual creep test. *Mech Mater* 2017b; **104**:49–59.
10. Ding XH, Ma T, Gu LH, et al. Discrete element methods for characterizing the elastic behavior of the granular particles. *J Test Evaluat* 2020b; **48**:20190178. doi: [10.1520/JTE20190178](https://doi.org/10.1520/JTE20190178).
11. Tang F, Zhu S, Xu G, et al. Influence by chemical constitution of aggregates on demulsification speed of emulsified asphalt based on UV-spectral analysis. *Construct Build Mater* 2019; **212**:102–8.
12. Tang FL, Ma T, Guan YS, Zhang ZX. Parametric modeling and structure verification of asphalt pavement based on BIM-ABAQUS. 2020a; **111**:103066. doi: [10.1016/j.autcon.2019.103066](https://doi.org/10.1016/j.autcon.2019.103066).
13. Tang FL, Ma T, Zhang JH, et al. Integrating three-dimensional road design and pavement structure analysis based on BIM. *Automat Construct* 2020b; **113**: <https://doi.org/10.1016/j.autcon.2020.103152>.
14. Zhang Y, Ma T, Luo X, et al. Prediction of dynamic shear modulus of fine aggregate matrix using discrete element method and modified Hirsch model. *Mech Mater* 2019a; **138**: 103148.
15. Reddy SS, Prasad ACSV, Krishna NV. Lime-stabilized black cotton soil and brick powder mixture as subbase material. *Adv Civ Eng Mater* 2018. doi: [10.1155/2018/5834685](https://doi.org/10.1155/2018/5834685).
16. Alhaji MM, Alhassan M. Effect of reclaimed asphalt pavement stabilization on the microstructure and strength of black cotton soil. *Int J Technol* 2018; **9**:727–36.
17. Yohanna P, Oluremi JR, Eberemu AO, et al. Reliability assessment of bearing capacity of cement-iron ore tailing blend black cotton soil for strip foundations. *Geotech Geol Eng* 2019; **37**:915–29.
18. Chen T, Ma T, Huang X, et al. The performance of hot-recycling asphalt binder containing crumb rubber modified asphalt based on physiochemical and rheological measurements. *Construct Build Mater* 2019; **226**: 83–93.
19. Zhu J, Ma T, Dong Z. Evaluation of optimum mixing conditions for rubberized asphalt mixture containing reclaimed asphalt pavement. *Construct Build Mater* 2020b; **234**:117426. doi: [10.1016/j.conbuildmat.2019.117426](https://doi.org/10.1016/j.conbuildmat.2019.117426).
20. Sani JE, Yohanna P, Etim KR, et al. Reliability evaluation of optimum moisture content of tropical black clay treated with locust bean waste ash as road pavement sub-base material. *Geotech Geol Eng* 2017; **35**:2421–31.
21. Zhu J, Ma T, Fang Z. Characterization of agglomeration of reclaimed asphalt pavement for cold recycling. *Construct Build Mater* 2020a; **240**:117912. doi: [10.1016/j.conbuildmat.2019.117912](https://doi.org/10.1016/j.conbuildmat.2019.117912).
22. Gobinath R, Ganapathy GP, Akinwumi II, et al. Plasticity, strength, permeability and compressibility characteristics of black cotton soil stabilized with precipitated silica. *J Cent South Univ* 2016; **23**:2688–94.
23. Ma T, Wang H, Zhang D, Zhang Y. Heterogeneity effect of mechanical property on creep behavior of asphalt mixture based on micromechanical modeling and virtual creep test. *Mech Mater* 2017a; **104**:49–59.

24. Ikeagwuani CC, Obeta IN, Agunwamba JC. Stabilization of black cotton soil subgrade using sawdust ash and lime. *Soils Found* 2019; **59**:162–75.
25. Jairaj C, Kumar MTP, Raghunandan ME. Compaction characteristics and strength of BC soil reinforced with untreated and treated coir fibers. *Innov Infrastruct So* 2018; **3**. doi: [10.1007/s41062-017-0123-2](https://doi.org/10.1007/s41062-017-0123-2).
26. Patel S, Shahu JT. Engineering properties of black cotton soil-Dolime mix for its use as subbase material in pavements. *Int J Geomate* 2015; **8**:1159–66.
27. Dalal SP, Patel R, Dalal PD. Effect on engineering properties of black cotton soil treated with agricultural and industrial waste. *Mater Today-Proc* 2017; **4**:9640–4.
28. Jimoh IO, Amadi AA, Ogunbode EB. Strength characteristics of modified black clay subgrade stabilized with cement kiln dust. *Innov Infrastruct So* 2018; **3**. doi: [10.1007/s41062-018-0154-3](https://doi.org/10.1007/s41062-018-0154-3).
29. Chen T, Luan YH, Ma T, et al. Mechanical and microstructural characteristics of different interfaces in cold recycled mixture containing cement and asphalt emulsion. *J Clean Prod* 2020; **258**:120674. doi: [10.1016/j.jclepro.2020.120674](https://doi.org/10.1016/j.jclepro.2020.120674).
30. Ma T, Zhang D, Zhang Y, Huang X. Effect of air voids on the high-temperature creep behavior of asphalt mixture based on three-dimensional discrete element modeling. *Mater Design* 2015b; **89**:304–13.
31. Tao Ma, Deyu Zhang, Yao Zhang, Siqi Wang, Xiaoming Huang, Simulation of wheel tracking test for asphalt mixture using discrete element modelling, *Road Mater Pavement Design*, 2018b, **19**(2): 367–384.
32. Zhang Y, Ma T, Luo X, et al. Prediction of Dynamic Shear Modulus of Fine Aggregate Matrix Using Discrete Element Method and Modified Hirsch Model. *Mech Mater* 2019d; **138**:103148. doi: [10.1016/j.mechmat.2019.103148](https://doi.org/10.1016/j.mechmat.2019.103148).
33. Ding X, Ma T, Zhang W, Zhang D. Experimental study of stable crumb rubber asphalt and asphalt mixture. *Construct Build Mater* 2017; **157**:975–81.
34. Ding XH, Ma T, Gu LH, Zhang Y. Investigation of Surface Micro-crack Growth Behavior of Asphalt Mortar Based on The Designed Innovative Mesoscopic Test. *Mater Design* 2019a; **185**:108238. doi: [10.1016/j.matdes.2019.108238](https://doi.org/10.1016/j.matdes.2019.108238).
35. Xunhao Ding, Tao Ma, Xiaoming Huang. Discrete-element contour-filling modeling method for micromechanical and macromechanical analysis of aggregate skeleton of asphalt mixture. *J Transport Eng, Part B: Pavements*, 2019b, **145**(1): 04018056. doi: [10.1061/JPEODX.0000083](https://doi.org/10.1061/JPEODX.0000083)
36. Yao Zhang, Tao Ma, Meng Ling, Deyu Zhang, Xiaoming Huang. Predicting dynamic shear modulus of asphalt mastics using discretized-element simulation and reinforcement mechanisms, *J Mater Civil Eng*, 2019c, **31**(8): 04019163. doi: [10.1061/\(ASCE\)MT.1943-5533.0002831](https://doi.org/10.1061/(ASCE)MT.1943-5533.0002831)
37. Ma T, Huang X, Zhao Y, Zhang Y. Evaluation of the diffusion and distribution of the rejuvenator for hot asphalt recycling. *Construct Build Mater* 2015c; **98**:530–6.
38. Tao Ma, Hao Wang, Liang He, Yongli Zhao, Xiaoming Huang, Jun Chen, Property characterization of asphalt and mixtures modified by different crumb rubbers, *J Mater Civil Eng*, 2017c, **29**(7): 04017036-1-10.
39. Zhang Y, Ma T, Ding X, et al. Impacts of air-void structures on the rutting tests of asphalt concrete based on discretized emulation. *Construct Build Mater* 2018; **166**:334–44.
40. Fredlund DG, Rahardjo H. *Soil mechanics for unsaturated soils*. New York: John Wiley and Sons, 1993
41. He ZY, Shen Y, Huang W, et al. Study on semi-rigid pavement structure with granular base. *Chin J Geotech Eng* 1998; **20**:93–6.
42. Ma T, Zhang D, Zhang Y, et al. Simulation of wheel tracking test for asphalt mixture using discrete element modelling. *Road Mater Pavement Des* 2018a; **19**:367–84.
43. Ding Xunhao, Chen Luchuan, Ma Tao, Ma Hai Xia, Gu Linhao, Chen Tian, Ma Yuan, Laboratory investigation of the recycled asphalt concrete with stable crumb rubber asphalt binder. *Construct Build Mater*, 2019, **203**: 552–557.
44. Yao Zhang, Tao Ma, Meng Ling, Xiaoming Huang. Mechanistic sieve-size classification of aggregate gradation by characterizing load-carrying capacity of inner structures, *J Eng Mech*, 2019b, **145**(9): 04019069-1-10. doi: [10.1061/\(ASCE\)EM.1943-7889.0001640](https://doi.org/10.1061/(ASCE)EM.1943-7889.0001640)